



Silica accelerates the selective hydrogenation of CO₂ to methanol on cobalt catalysts

Lingxiang Wang ^{1,2,7}, Erjia Guan^{3,7}, Yeqing Wang^{2,7}, Liang Wang^{1,4}✉, Zhongmiao Gong⁵, Yi Cui ⁵, Xiangju Meng², Bruce C. Gates³ & Feng-Shou Xiao^{1,2,6}✉

The reaction pathways on supported catalysts can be tuned by optimizing the catalyst structures, which helps the development of efficient catalysts. Such design is particularly desired for CO₂ hydrogenation, which is characterized by complex pathways and multiple products. Here, we report an investigation of supported cobalt, which is known for its hydrocarbon production and ability to turn into a selective catalyst for methanol synthesis in CO₂ hydrogenation which exhibits good activity and stability. The crucial technique is to use the silica, acting as a support and ligand, to modify the cobalt species via Co–O–SiO_n linkages, which favor the reactivity of spectroscopically identified *CH₃O intermediates, that more readily undergo hydrogenation to methanol than the C–O dissociation associated with hydrocarbon formation. Cobalt catalysts in this class offer appealing opportunities for optimizing selectivity in CO₂ hydrogenation and producing high-grade methanol. By identifying this function of silica, we provide support for rationally controlling these reaction pathways.

¹Key Lab of Biomass Chemical Engineering of Ministry of Education, College of Chemical and Biological Engineering, Zhejiang University, 310027 Hangzhou, China. ²Key Laboratory of Applied Chemistry of Zhejiang Province, Department of Chemistry, Zhejiang University, 310028 Hangzhou, China. ³Department of Chemical Engineering, University of California, Davis, CA 95616, United States. ⁴Zhejiang Provincial Key Laboratory of Advanced Chemical Engineering Manufacture Technology, Zhejiang University, 310027 Hangzhou, China. ⁵Vacuum Interconnected Nanotech Workstation (Nano-X), Suzhou Institute of Nano-Tech and Nano-Bionics (SINANO), Chinese Academy of Sciences (CAS), 215123 Suzhou, China. ⁶Beijing Advanced Innovation Center for Soft Matter Science and Engineering, Beijing University of Chemical Technology, 100029 Beijing, China. ⁷These authors contributed equally: Lingxiang Wang, Erjia Guan, Yeqing Wang. ✉email: liangwang@zju.edu.cn; fsxiao@zju.edu.cn

The increasing atmospheric CO₂ concentration originating from anthropogenic emissions has caused global warming and related climate issues. Progress to reduce fossil fuel consumption and reduce CO₂ emissions is substantial but insufficient, and research is underway to develop processes for large-scale CO₂ sequestration, but validated technology is still lacking. Additional prospects for CO₂ reduction on a significant scale include processes for conversion of CO₂ as a feedstock for manufacture of platform chemicals and fuels, including CO^{1,2}, olefins^{3,4}, alcohols^{5–8}, and hydrocarbon fuels^{9–11}. The most promising candidate routes are catalytic, including the hydrogenation of CO₂ to produce methanol, a large-scale platform chemical for the production of olefins, gasoline, aromatics¹², and other chemicals¹³. Further, methanol is a fuel in its own right and also promising for the storage of hydrogen¹⁴, with the prospect of playing a significant role in hydrogen fuel cells¹⁵. The CO₂-to-methanol transformation is challenging because of the chemical inertness of CO₂ and the difficulty of converting it selectively to desired products.

Catalysts for the hydrogenation of CO₂ to methanol include supported Au particles¹⁶, In₂O₃¹⁷, Ni–Ga¹⁸, Pd–Ga¹⁹, Zn–Zr²⁰, and Mn–Co²¹. Copper, which has the advantage of being earth-abundant, has been widely investigated and applied^{22–28}. Numerous copper catalysts have been designed recently to optimize interfaces between copper and metal oxide supports, because copper alone is less effective in bonding and activating CO₂; successful examples include Cu/ZnO/Al₂O₃ (used industrially for hydrogenation of CO and CO₂)^{22–25}, Cu/ZrO₂²⁶, Cu/CeO₂²⁷, and Cu/TiO₂²⁸. In these cases, a wide scope of reaction intermediates and pathways have been identified by using the supported copper as models^{22–24,26,28}, but how to optimize the catalyst structure for turning the selectivity is still in need of investigation. In addition, supported copper usually suffers from deactivation caused by nanoparticle sintering under harsh reaction conditions^{29,30}.

Consequently, researchers have been motivated to find replacements for supported copper catalysts, focusing on inexpensive and earth-abundant metals that work effectively, such as cobalt. Cobalt is widely used in industry as a catalyst for Fischer–Tropsch synthesis³¹, also drawing attention for CO oxidation³² and ammonia synthesis³³. But cobalt is regarded as inappropriate for the selective methanol formation, because of its high activity for C–O dissociation³⁴, and CO and hydrocarbons usually form rather than methanol³⁵. On the other hand, recent efforts on selectivity optimization in CO₂ hydrogenation have focused on engineering metal oxide supports with redox properties and electronic metal–support interactions^{1,2,36–38}, but the promotion role of inert supports, such as silica, has been largely overlooked.

Herein, we report how cobalt can be optimized to give efficient catalysts for methanol production by choice of a silica support. The catalyst is synthesized by incorporating cobalt nanoparticles onto amorphous silica (Co@Si_x) to construct abundant Co–O–SiO_n interfaces, which stabilize methoxy (*CH₃O) species as intermediates in CO₂ hydrogenation. Optimizing the cobalt-to-silica ratio gives superior catalysts, even outperforming those expensive noble-metal catalysts¹⁹ as well as the supported copper catalysts^{25,28} employed for hydrogenating CO₂ to methanol.

Results

Synthesis. The method for synthesizing Co@Si_x is summarized in Fig. 1. To construct the Co–O–SiO_n linkage, the hydrolysis of tetraethoxysilane (TEOS) was performed in a basic liquor containing Co(NO₃)₂, followed by calcination of the resultant solid at 500 °C to form a product containing predominantly Co₃O₄, as shown by X-ray diffraction (XRD) crystallography (Co₃O₄@Si_x,

Supplementary Fig. 1). The final product was obtained by reduction with hydrogen at 600 °C. The composition was adjusted by changing the amount of TEOS in the starting solution, giving Co@Si_x, where *x* is the molar ratio of silica to cobalt (Supplementary Tables 1 and 2). For comparison, a conventional catalyst consisting of cobalt nanoparticles supported on silica (Co/SiO₂) was synthesized by a deposition method (details in the SI), the cobalt loading was 43 wt%.

Catalysis in CO₂ hydrogenation. Fig. 2 shows the performance of a set of cobalt catalysts in CO₂ hydrogenation with a feed gas at a pressure of 2.0 MPa containing CO₂ and H₂ (H₂/CO₂ = 3:1, molar). The products, besides methanol, were CO and methane, formed respectively by the reverse water-gas shift and methanation reactions. A cobalt catalyst without silica (CoO_x) was characterized under our conditions by a CO₂ conversion of 6.7%, with CO and methane as the dominant products, and a slight amount of methanol (Fig. 2a). Significantly, the inclusion of silica in the cobalt catalyst improved both the CO₂ conversion and methanol selectivity. For example, the Co@Si_{0.52} catalyst gave CO₂ conversion and methanol selectivity of 9.0% and 47.9%, respectively. The methanol selectivity was further optimized by changing the cobalt/silica ratio, with the methanol selectivity of 70.5% at a CO₂ conversion of 8.6% for Co@Si_{0.95} (Supplementary Table 1, Fig. 2b and c). In the catalytic reaction experiment, methanol was the sole carbon-containing liquid product (condensed in a cold trap downstream of the reactor) without any C₂₊ by-products, which are usually formed in conversions with cobalt-containing catalysts^{5,7}, revealing a potentially valuable methanol production process.

In contrast, more silica in the catalyst led to decreased CO₂ conversions and lower methanol selectivity, illustrated by data characterizing the performance of Co@Si_{1.48} and Co@Si_{1.87}, which might be due to changes in the state of cobalt and/or blocking of cobalt active sites by silica. In contrast, the conventional cobalt catalyst (Co/SiO₂) gave a CO₂ conversion of 7.3% and a methanol selectivity at 16.6%, with CO being the dominant product under the equivalent reaction conditions. These data confirm the unusual catalytic performance of Co@Si_{0.95} in the CO₂ hydrogenation.

As expected, increased operating temperatures of the Co@Si_{0.95} catalyst (Supplementary Fig. 4) gave higher conversions, with the methanol selectivity being >70% at 260–320 °C but decreasing at temperatures >320 °C. Similar trends were observed with the other Co@Si_x catalysts (Supplementary Figs. 2–7). In these cases, the Co@Si_x catalysts exhibited a marked decrease in selectivity to the undesired methane compared with the conventional cobalt catalysts (Supplementary Fig. 8). The conventional Co/SiO₂ was characterized by methanol selectivity generally <25% at temperatures in the range of 260–380 °C (Supplementary Figs. 9 and 10), where the C₂₊ hydrocarbons were also detected with selectivity of 4.0%–8.5% at 260–380 °C. As shown in Fig. 2b, Co@Si_{0.95} catalyst gave methanol productivity of 3.0 mmol g_{cat}^{−1} h^{−1}, outperforming Co/SiO₂ and even the other supported copper and noble-metal catalysts that have been reported to be excellent for the CO₂-to-methanol transformation (Supplementary Table 3)^{19,25,28}. For example, the methanol productivity of Co@Si_{0.95} was found to be comparable to that of Cu/SiO₂ under comparable conditions³⁹.

The conventional supported metal nanoparticle catalysts generally suffer from the poor stability^{29,30}. For example, the standard commercial Cu/ZnO/Al₂O₃ catalyst (Supplementary Figs. 11–13) for synthesis of methanol from CO₂ hydrogenation, evaluated in a wide temperature range (200–380 °C, Supplementary Fig. 12), gave the performances that are sensitive to the reaction temperatures. The best methanol yield appeared at

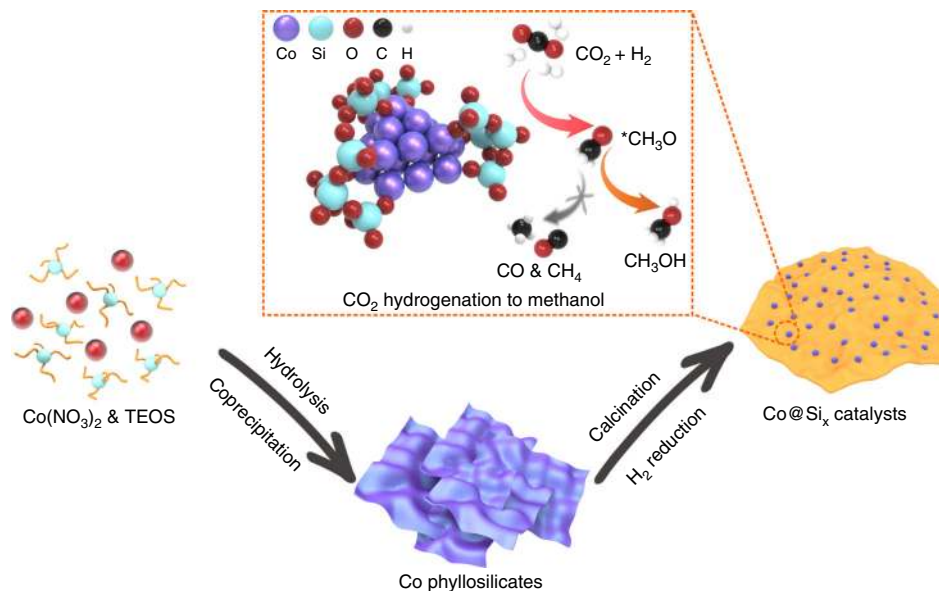


Fig. 1 Synthesis and catalysis strategies of Co@Si_x catalysts. The procedures with cobalt phyllosilicates as intermediates for synthesizing Co@Si_x. Within the highlighted square, the CO₂-to-methanol transformation on Co@Si_x catalysts.

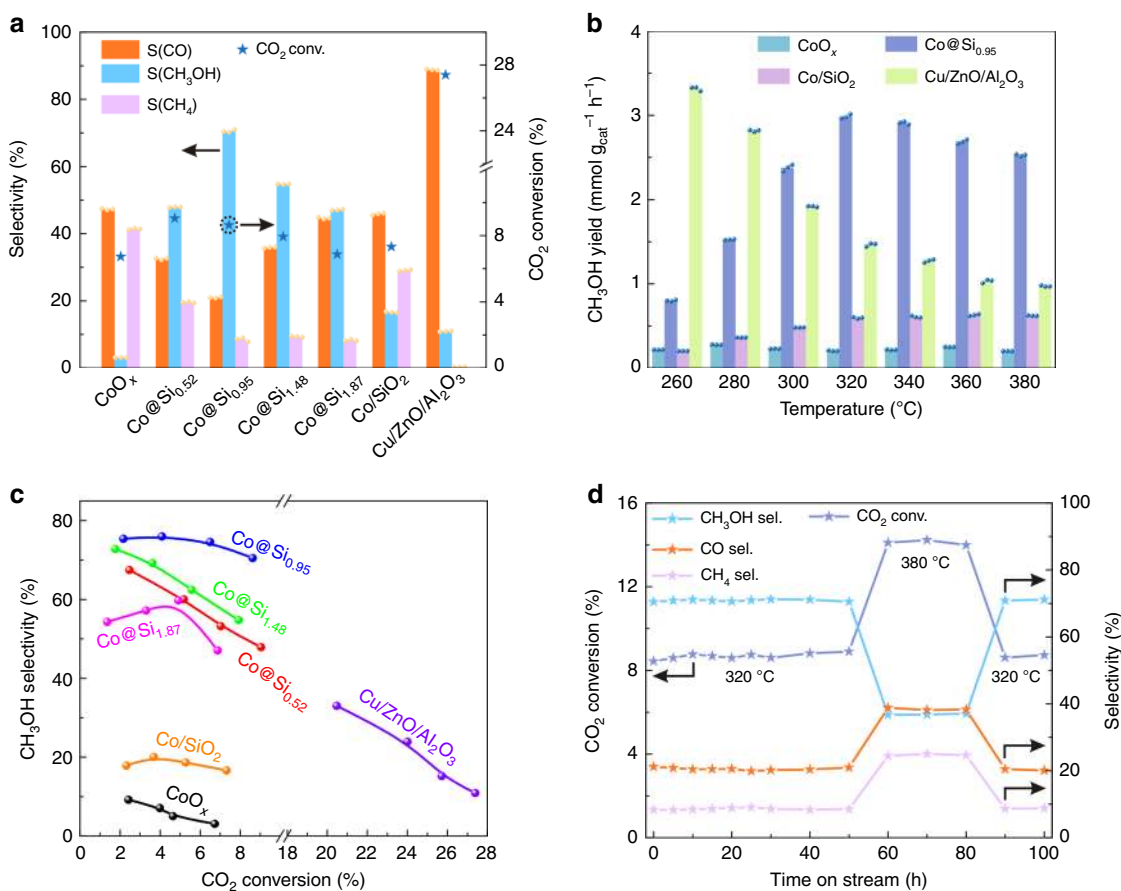


Fig. 2 Performance of Co@Si_x catalysts in CO₂ hydrogenation. **a** Performance of catalysts, standard reaction conditions for Co@Si_{0.95}: 0.2 g of catalyst, pressure = 2.0 MPa; H₂/CO₂ feed ratio = 3:1, molar; temperature = 320 °C; GHSV = 6000 mL/g h. The mass of the other Co@Si_x catalysts was chosen to give the same cobalt content in the reactor. **b** Dependences of methanol yield on temperature. Each reaction was performed three times, and the corresponding data points are provided in the bar charts. Error bounds for the conversion and selectivity are ± 0.3% and ± 0.5%, respectively. **c** CO₂ conversion and CH₃OH selectivity of Co@Si_x catalysts at 260–320 °C. **d** Stability test of Co@Si_{0.95} catalyst operated for 100 h in a flow reactor.

240 °C, giving productivity of 3.5 mmol $g_{\text{cat}}^{-1} h^{-1}$ with CO₂ conversion of 15.2% and methanol selectivity of 47.6%, which is higher than that of the Co@Si_{0.95} catalyst (3.0 mmol $g_{\text{cat}}^{-1} h^{-1}$). However, the Cu/ZnO/Al₂O₃ was characterized by a markedly inferior performance in the reaction life test, losing almost half of the methanol yield after reaction at 240 °C for 50 h (Supplementary Fig. 13). This result is in agreement with the knowledge of the Cu/ZnO/Al₂O₃ catalyst, whereby the Cu nanoparticles easily sinter into larger ones and cause deactivation^{29,30}. Significantly, Co@Si_{0.95} underwent almost negligible decay in the CO₂ conversion and methanol selectivity in 100 h of onstream operation (70 h at 320 °C and 30 h at 380 °C, Fig. 2d).

To the best of our knowledge, this excellent performance of Co@Si_{0.95} catalyst in the CO₂ hydrogenation to methanol is unmatched. We are led to hypothesize that the silica support plays a key role, because the comparable silica-supported catalyst, Co/SiO₂, did not show this behavior. We were thus motivated to investigate the catalysts in depth and to determine catalytic structure-performance relationships.

Catalyst structure study. A transmission electron microscopy (TEM) image of Co@Si_{0.95} (Fig. 3a) shows a lamellar structure of cobalt phyllosilicates. A high-angle annular dark field scanning transmission electron microscopy image (HAADF-STEM, Fig. 3b) and EDX elemental maps (Fig. 3c–e) demonstrate uniform dispersions of cobalt and silicon. The TEM image of Fig. 3f shows cobalt nanoparticles with an average diameter of 3.9 nm supported on the silica. A high-resolution TEM (HRTEM) image reveals the co-existence of metallic Co and CoO phases on the cobalt nanoparticles present in Co@Si_{0.95} (Fig. 3g), which is further confirmed by the fast Fourier-transform (FFT) analysis (Fig. 3h) and XRD patterns. The cobalt nanoparticles on a series of Co@Si_x samples have similar diameters, as evidenced by the HRTEM characterization. In contrast, the CoO_x and Co/SiO₂ catalysts incorporate metallic Co as the dominant phase

(Supplementary Figs. 14–18). These data indicate a role of silica controlling the dispersion and the oxidation state of cobalt.

The cobalt-silica interaction on Co@Si_x samples was investigated with FT-IR spectroscopy, with the bands at 665 and 1025 cm⁻¹, assigned to the Co–O–Si_n linkage (Fig. 3i and Supplementary Fig. 19)⁴⁰. In contrast, these bands are undetectable in the FT-IR spectrum of Co/SiO₂, consistent with the lack of substantial interactions between cobalt and silica. X-ray absorption near edge structure (XANES) and extended X-ray absorption fine structure (EXAFS) spectra were recorded to characterize the oxidation states and coordination environments of Co in the Co@Si_x samples. The Co K-edge XANES spectra of Co@Si_x samples exhibit pre-edge features of the Co 1s–3d absorption transition at 7709.5 eV, with absorption edge positions of 7721.6 ± 0.2 eV (Fig. 3j and Supplementary Fig. 20)—these features are characteristic of cobalt oxides⁴¹. In contrast, the Co K-edge XANES of Co/SiO₂ is represented by an edge position of 7709.0 eV, assigned to metallic cobalt. These results point to the presence of cationic cobalt bonded to the silica, with Co–O–Si_n linkages at the Co–SiO₂ interfaces stabilizing the dispersed cobalt species in Co@Si_x. X-ray absorption spectra (XAS) recorded at the O K-edges of Co@Si_x provide evidence confirming the hypothesis: the spectra include peaks assigned to Co–O bonds, at 532.5 and 539.8 eV⁴², whereas the Co/SiO₂ exhibits an extremely weak Co–O signal because of its metallic feature (Supplementary Fig. 21).

In contrast, EXAFS spectra of Co/SiO₂, recorded at the Co K-edge (Fig. 3k), include a Co–Co shell with a distance determined in the fitting to be 2.50 Å, with a coordination number of 9.3, indicating the dominant presence of metallic cobalt (Supplementary Table 4). Consistent with our interpretation, the Co–Co contributions characteristic of metallic cobalt are extremely weak in the spectra of Co@Si_x samples. The EXAFS spectra indicate Co–O and Co–Co shells at distances of 2.05 and 3.02 Å, respectively, for Co@Si_{0.95}, with coordination numbers of 4.2 and 10.7, consistent with the presence of nonmetallic cobalt bonded to silica.

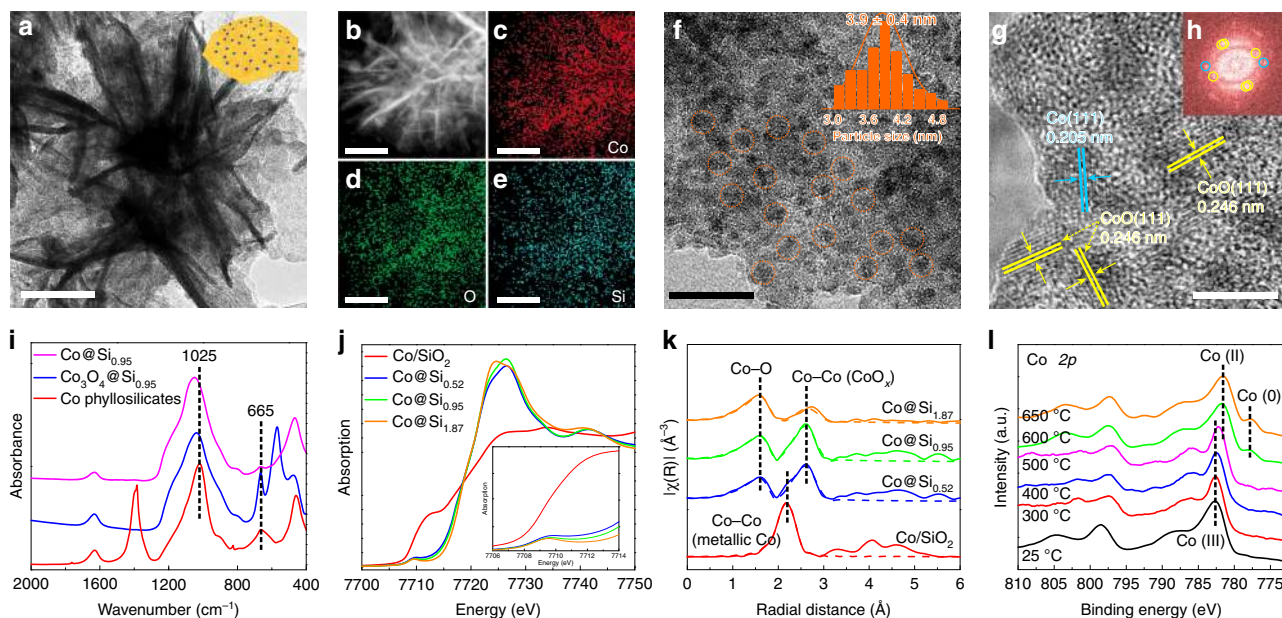


Fig. 3 Structural characterization of Co@Si_{0.95} catalyst. **a** TEM image of Co@Si_{0.95}. **b–e**, **b** HAADF-STEM image and EDX elemental maps of **c** Co, **d** O, and **e** Si of Co@Si_{0.95}. **f, g** HRTEM images of Co@Si_{0.95}. The orange circles highlight the Co nanoparticles (inset of **f**: size distribution of Co nanoparticles.) **h** FFT image of the Co nanoparticles corresponding to the HRTEM image in **g**. Scale bars: 100 nm in **a–e**, 20 nm in **f**, and 5 nm in **g**. **i** FT-IR spectra of Co@Si_{0.95} samples. **j, k** Co K-edge X-ray absorption spectra. **j** XANES spectra (inset: enlarged pre-edge region) and **k** EXAFS spectra with k^2 -weighted data (solid line) and fit corresponding to recommended model (dashed line) of Co@Si_x and Co/SiO₂ samples. **l** In situ Co 2p XPS spectra of Co₃O₄@Si_{0.95} under 0.1 mbar of H₂ at various temperatures.

To further characterize these dispersed cobalt species, we did in situ Co 2p XPS experiments with the samples undergoing reductive treatments (Fig. 31 and Supplementary Figs. 22–25). The as-synthesized Co₃O₄/Si_{0.95} sample was characterized by a dominant signal assigned to Co³⁺ (782.4 eV, Supplementary Fig. 26), which was resistant to reduction and unchanged even after exposure to H₂ at 500 °C. Reduction at 600 and 650 °C gave spectra indicating the predominant presence of Co²⁺ (781.5 eV) with some Co⁰ (777.8 eV), indicating that the surface of Co@Si_{0.95} incorporated predominantly cobalt oxide species and a small amount of metallic cobalt after vigorous reduction. Although the in situ XPS was performed using hydrogen with a lower pressure than that of the practical reduction treatment because of the XPS technique limitation⁴³, it is sufficient to reduce the cobalt species. For example, the Co³⁺ on Co₃O₄/SiO₂ was easily reduced to Co²⁺ at a temperature of only 300–400 °C, and Co⁰ was the only cobalt species detected after reduction at 500 and 600 °C (Supplementary Figs. 27 and 28). This result is in good agreement with the H₂-TPR measurement of the cobalt oxide sample (Supplementary Fig. 29). These results all support the conclusion that the cobalt species in Co@Si_x are strongly resistant to reduction.

In order to provide more evidence, we treated the Co@Si_{0.95} sample with relatively high-pressure H₂ at 600 °C for 2 h (10% H₂ in Ar, 2 MPa), which should provide enough hydrogen for reducing the cobalt species. Significantly, the treated Co@Si_{0.95} still contained cobalt oxide as the dominant phase with a small amount of metallic cobalt, as confirmed by the XRD (36.4°, 42.5° and 61.5° assigned to CoO phase) and XPS characterizations (781.5 eV assigned to Co²⁺ and 777.8 eV assigned to Co⁰) (Supplementary Fig. 30). The conclusion is further confirmed by in situ Raman spectra (Supplementary Fig. 31). By increasing reduction temperature to 600 °C, Co@Si_x samples still showed a typical Raman signal of Co–O species, which was undetectable on the reduced Co/SiO₂. Even after reaction for 100 h under the practical CO₂ hydrogenation conditions (Fig. 2d), the Co@Si_{0.95} sample still exhibited the dominant CoO phase with a relatively small amount of metallic Co (XRD and XPS in Supplementary Fig. 32), confirming the difficult-to-reduce cobalt species on the Co@Si_{0.95} catalyst, in good agreement with the in situ XPS investigation.

On the basis of these results, we propose that the silica influences the cobalt oxidation state, resulting in structures that are active and selective catalysts for methanol formation and not for methane and CO formation³⁵. The relationships between the methanol yield in CO₂ hydrogenation and Co⁰/Co²⁺ ratio for various catalysts are presented in Supplementary Fig. 24f. Compared with CoO_x catalyst, the Co@Si_{0.52} and Co@Si_{0.95} with Co²⁺ species exhibited enhanced methanol yields. Further decreasing the Co⁰/Co²⁺ ratio reduced the methanol yields over Co@Si_{1.48} and Co@Si_{1.87} catalysts. These data confirm the balanced metallic Co and CoO phases on the catalysts are important for the methanol production. More Co⁰ species cause the formation of a large amount of methane with poor methanol selectivity. Consistent with this picture, the hydrogen dissociation ability was evaluated by the catalysis in HD production by the reaction of H₂ with D₂ (a measurement of activity for activation of dihydrogen) over the Co/SiO₂ and Co@Si_{0.95} catalysts. The product of the former contained 85% HD and only 27% HD for the latter (Supplementary Fig. 33), suggesting the H₂ dissociation ability of Co@Si_{0.95} was weakened because such ability was strongly related to the metallic Co. The surprising finding is that the Co@Si_{0.95} with lower H₂ dissociation ability even exhibits higher CO₂ conversions than the Co/SiO₂ catalysts with high activity in H₂ activation. The sole CoO phase is known to have poor activity for the hydrogenation. Therefore, the Co@Si_{0.95} catalyst with balanced phases exhibited the best performance

among these samples (Supplementary Figs. 34–36). Apart from influencing the cobalt oxidation state, more silica species might block more surface sites of the Co@Si_x catalysts, which would also influence the catalytic performance. These data might explain why the various Co@Si_x catalysts with similar cobalt nanoparticle sizes have markedly different catalytic performance.

We conclude that the silica acts as an effective support for turning the cobalt nanoparticles from catalysts for methanation/CO formation into catalysts for methanol production, exhibiting simultaneously high activity, selectivity, and durability for the CO₂-to-methanol transformation. Such different catalytic features are associated with the Co–O–SiO_n linkage. It is reasonable to understand this linkage stabilizes the cobalt nanoparticles and hinders the sintering during the calcination/reduction/reaction under harsh conditions. For example, after reaction for 100 h, the used Co@Si_{0.95} catalyst still incorporated the cobalt nanoparticles with an average diameter of 3.9 nm, which is almost unchanged compared with the as-synthesized catalyst (Supplementary Fig. 37). The Co₂C/CoC species are undetectable on Co@Si_{0.95} as confirmed by the XRD pattern and HRTEM images (Supplementary Figs. 32 and 37). In contrast, the used Co/SiO₂ contained predominantly metallic Co accompanied by Co₂C species (Supplementary Figs. 38 and 39) after the equivalent test for 100 h, in good agreement with expectation^{44,45}. The remarkably different phenomena of Co@Si_{0.95} compared with the conventional cobalt catalysts are attributed to the Co–O–Si linkage on the Co@Si_{0.95} catalyst, which hindered the carbonization of cobalt species^{46,47}.

Mechanism study. In order to gain insight into how the silica modification influences the reaction pathways, we characterized the samples using IR spectroscopy in CO₂ adsorption and hydrogenation. Supplementary Fig. 40 shows the spectra of various catalysts after exposure to CO₂, with the CoO_x characterized by bands at 1260, 1530, 2850, 2945, and 3015 cm⁻¹, assigned to carboxylate (CO₂^{δ-}, 1260 cm⁻¹), formate (*HCOO, 1530, 2850, and 2945 cm⁻¹), and *CH_x species (3015 cm⁻¹), respectively^{28,48–50}. The CO₂^{δ-} is from the chemisorbed CO₂ species on the cobalt sites, and the *HCOO and *CH_x are from the interaction of chemisorbed CO₂ with hydrogen adatom on cobalt sites resulted from the H₂ pretreatment. The *CH_x species, which are known intermediates in methane formation, confirm that deep hydrogenation occurs on the CoO_x catalyst⁵⁰. It is significant that the *CH_x band (3015 cm⁻¹) was almost undetectable in the spectra of the Co@Si_x catalysts, consistent with the suppression of deep hydrogenation of CO₂ which requires metallic sites³⁵. The spectra further show that more silica species in Co@Si_x correspond to lower intensity of *HCOO (2850 and 2945 cm⁻¹), also being correlated with those of the chemisorbed CO₂ (CO₂^{δ-}, 1244–1276 cm⁻¹).

To identify reaction intermediates, we collected in situ DRIFTS spectra (Fig. 4a and Supplementary Figs. 41–43), bringing the catalysts in contact with feed gases having varied CO₂ and H₂ concentration at 350 °C. Exposure of Co@Si_{0.95} to CO₂ without H₂ gave rise to bands, mainly including those of CO₂^{δ-} (1246, 1592 cm⁻¹), CO₃²⁻ (1435 cm⁻¹), and *HCOO (1337, 2850, 2945 cm⁻¹)²⁸. When H₂ was present (CO₂:H₂, molar ratio = 3), the bands of CO₂^{δ-} (1246, 1592 cm⁻¹) were markedly weakened and those of *HCOO (1360, 1560 cm⁻¹) enhanced. Simultaneously, new bands appeared at 1048, 1462, 2830, and 2928 cm⁻¹, assigned to *CH₃O species. Continuous feeding of H₂ (switch off CO₂) markedly increased the *HCOO and *CH₃O band intensities (Fig. 4b, 0–12 min). After 12 min, the *HCOO signal was constant, but the *CH₃O signal continued

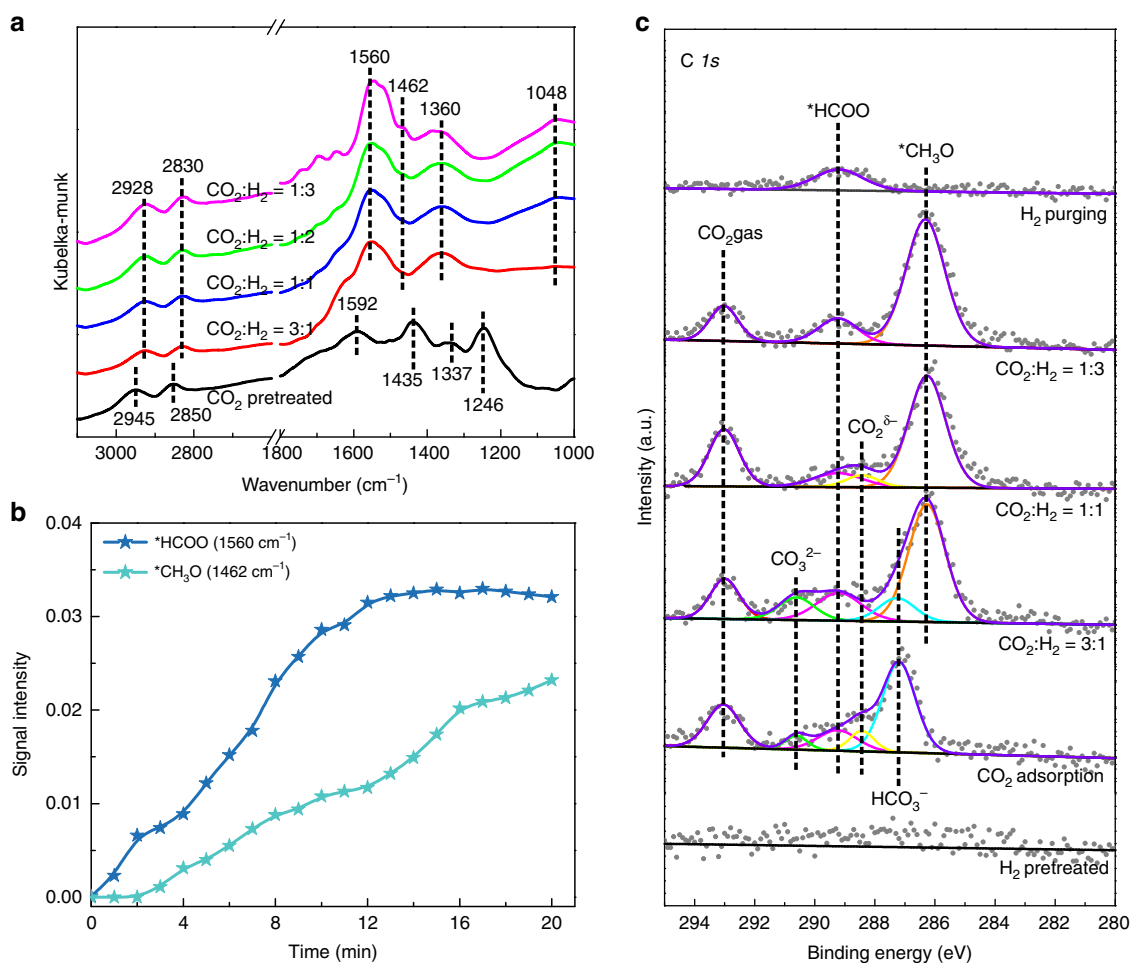


Fig. 4 Mechanism of CO₂ hydrogenation on Co@Si_{0.95} catalyst. **a** In situ DRIFTS spectra of Co@Si_{0.95} catalyst at 350 °C in contact with CO₂ + H₂. **b** Time-dependent DRIFTS band intensities characterizing surface *HCOO and *CH₃O species during the CO₂ + H₂ reaction on Co@Si_{0.95} at 350 °C. **c** In situ C 1s XPS spectra of Co@Si_{0.95} in contact with 1.2 mbar of CO₂ + H₂ atmosphere with controlled ratios at 250 °C.

to increase. In contrast with the spectra of Co@Si_{0.95}, the comparable spectra Co/SiO₂ and CoO_x give evidence of only trace of *CH₃O (in contrast to the stronger bands of *HCOO and/or *CH_x species). The *CH₃O species are readily converted into methanol by hydrogenation^{22,24}, and the high methanol selectivity of Co@Si_{0.95} is ascribed to these species as reaction intermediates. The trace of *CH₃O signal on Co/SiO₂ and CoO_x is consistent with their low methanol selectivity.

Further investigation of the reaction intermediates on Co@Si_{0.95} was performed with ambient-pressure (AP) XPS. Although the CO₂ and H₂ pressure was much lower than that in the practical tests, it is sufficient to react with the catalyst surface. Changes in the surface and reaction intermediates were shown by X-ray photoelectron spectra^{16,27,50}. CO₂ is readily adsorbed on this catalyst, giving rise to C 1s bands at 293.0, 290.6, 289.2, 288.4, and 287.2 eV, assigned to gaseous CO₂, CO₃²⁻, *HCOO, CO₂^{δ-}, and HCO₃⁻ species, respectively (Fig. 4c)⁵¹. When the sample was exposed to H₂ (CO₂:H₂, molar ratio = 3), signals characteristic of CO₂^{δ-} and HCO₃⁻ were reduced and that of *HCOO enhanced. Concomitantly, a signal appeared at 286.3 eV and became dominant, indicating the formation of abundant *CH₃O species. More H₂ in the feed gas (CO₂/H₂ ratio = 1/3, molar) markedly reduced the bands of chemisorbed CO₂ (CO₂^{δ-} and CO₃²⁻), which were quickly transformed to *CH₃O species by feeding sufficient hydrogen, whereas the signal of *HCOO remained almost unchanged. When the feed gas was switched

to pure H₂ without CO₂, the *CH₃O signal disappeared immediately—this species was evidently further hydrogenated to form methanol. However, the *HCOO signal remained essentially constant, as this species was resistant to hydrogenation on the catalyst (Supplementary Figs. 44 and 45). In contrast, the Co/SiO₂ catalyst was also characterized by chemisorbed CO₂, but with extremely weak *CH₃O bands under the equivalent conditions (Supplementary Fig. 46), in good agreement with the DRIFTS spectra. These data confirm the importance of the silica-supported species containing cationic cobalt for *CH₃O formation and stabilization, even when the reaction atmosphere contains only little H₂ (CO₂/H₂, molar ratio = 10:1, Supplementary Figs. 47 and 48).

The easily detected abundant *CH₃O signals in the in situ DRIFTS and XPS characterization confirm the fast formation and slow further transformation of *CH₃O on the Co@Si_x catalyst (Supplementary Figs. 49 and 50). Apart from the hydrogenation to *CH₃OH, the *CH₃O species might also undergo C–O cleavage and the subsequent hydrogenation to CH₄^{24,28,52}, as well as the dehydrogenation to CO. With regard to the *CH₃O transformation, multiple reaction pathways have been proposed in the formation of *CH_x intermediates, that are ready to proceed the methanation⁵⁰. In this route, the C–O cleavage is always regarded to be the rate controlling step^{24,28,52}. Reported density functional theoretical calculations have revealed that the cleavage of the C–O bond in *CH₃O requires the metallic Co surface or the CoO

surface with abundant oxygen vacancies. The CoO(100) surface saturated with oxygen leads to a high energy barrier for the *CH_3O dissociation at 2.71 eV [1.45 eV for Co(111) surface and 1.01 eV for the oxygen vacancy-rich CoO(100)]³⁵. The Co@Si_{0.95} catalyst with not-easy-to-reduce oxygen species provided an ideal catalyst surface for hindering the C–O cleavage. In addition, the C–O bond cleavage is known to be assisted by hydrogen⁵³, and the relatively lower activity of Co@Si_{0.95} for dihydrogen activation (Supplementary Fig. 33) might also contribute to stabilization of *CH_3O intermediates to avoid C–O cleavage. Apart from the *CH_3O decomposition, another possible route for methane or other higher hydrocarbons formation is via the direct CO dissociation into *C species, which has been experimentally and theoretically studied in the cobalt-catalyzed Fischer–Tropsch synthesis^{31,54}. Metallic cobalt and cobalt carbide were found to be efficient for CO dissociation, but the oxidized cobalt surface is known to be less active, which is also confirmed by the poor activity of Co@Si_{0.95} in the CO hydrogenation (CO conversion of 0.7% and methanol selectivity of 22.7%) under the employed reaction conditions (360 °C, 2.0 MPa, Supplementary Fig. 51).

In addition to the C–O cleavage, another possible route for *CH_3O transformation is dehydrogenation, giving CO product. To probe this reaction, we performed temperature-programmed surface reaction (TPSR) experiments to evaluate the reaction of *CH_3O on different catalysts, with methanol as a feed because it easily forms *CH_3O species. As shown in Supplementary Fig. 52, the CO signal centered at 280 °C characterizing the Co/SiO₂ catalyst demonstrates the dehydrogenation of the *CH_3O species indeed occurred on the surface of metallic cobalt. In contrast, no CO signal was observed in equivalent experiments with the Co@Si_{0.95} catalyst at temperatures <300 °C, evidencing the enhanced ability of Co@Si_{0.95} catalyst to resist dehydrogenation. In addition to the CO, the methane signal was detected at 340 °C on Co/SiO₂ catalyst, attributed to the C–O dissociation and deep hydrogenation to methane. In contrast, no methane signal was observed on Co@Si_{0.95} catalyst, even at temperature up to 420 °C. These results might explain the reduced methanation and CO formation on the Co@Si_{0.95} catalyst, whereby the stabilization of *CH_3O species on the catalyst surface hinders the C–O cleavage and deep dehydrogenation. This feature contributes to the high methanol productivity via further hydrogenation of the *CH_3O intermediates, in good agreement with the XPS results (Supplementary Figs. 47c and 48c).

Discussion

A central result emerging from the in situ DRIFTS and XPS data is that the *CH_3O species on Co@Si_{0.95} act as intermediates for methanol formation. The observation of abundant *CH_3O species indicates that they are stable intermediates. The results suggest that the CO₂ hydrogenation on Co@Si_{0.95} might proceed by a mechanism similar to that occurring on the well-known Cu/ZnO catalyst²⁴, whereby the transformation of *CH_3O is crucial for the selective formation of methanol. Another central result is the catalyst performance data showing that methanol forms with much less accompanying CO and methane—their formation from *CH_3O would require deep dehydrogenation and breaking of the C–O bond, respectively, which readily occurs on metallic cobalt but not on the cobalt oxide surface with unreducible oxygen, according to the reported simulation results³⁵. Thus, we infer that the dominant cobalt oxide phase on Co@Si_{0.95} provides a nearly optimum structure for hindering the side reactions and facilitating methanol formation.

Catalysts in this class offer a compelling example showing the key role of a nominally inert support—silica—turning cobalt from a nonselective catalyst into highly selective catalyst for methanol

production. We suggest this work may open the way to new control of catalysts by supports and help guide the design of improved catalysts for selective hydrogenation of CO₂.

Methods

Materials. Co(NO₃)₂·6H₂O (99.0%), Co₃O₄ (99.5%, 100 nm), CO(NH₂)₂ (99.5%), and tetraethylorthosilicate (TEOS, 99.0%) were obtained from Aladdin Chemical Reagent Company. NaOH (96.0%), NH₃·H₂O (25.0%–28.0%) and amorphous SiO₂ were obtained from Shanghai Lingfeng Chemical Reagent Co. Ltd. Cu/ZnO/Al₂O₃ was provided by Beijing Sanju Environmental Protection & New Materials Co. Ltd. Pure Ar, CO, CO₂, CH₄, 10% H₂/Ar, 10% CO₂/Ar, CO₂/H₂/Ar (25%/50%/25%, 20%/60%/20%), and 19%/76%/5%) and CO/H₂/Ar (30%/60%/10%) were provided by Hangzhou Jingong Special Gases Co. Ltd.

Catalysts preparation. Synthesis of Co₃O₄@Si_{0.95} and Co@Si_{0.95} catalysts: The Co (NO₃)₂·6H₂O (40 mmol) and TEOS (40 mmol) were dissolved in 200 mL mixed liquor containing water and ethanol with the volume ratio of 3/1, followed by adding 20 mL of NH₃·H₂O. After stirring at room temperature for another 8 h, the precipitate was separated by filtration, washed with deionized water, and dried at 100 °C overnight to obtain Co phyllosilicates. The Co₃O₄@Si_{0.95} was obtained by calcining the Co phyllosilicates at 500 °C in air for 4 h. After reducing Co₃O₄@Si_{0.95} in flowing hydrogen (10% H₂/Ar, 60 mL/min) for 3 h at 600 °C, the Co@Si_{0.95} catalyst was obtained.

Synthesis of Co₃O₄@Si_x and Co@Si_x catalysts with different Si/Co ratios: The Si/Co ratio was adjusted to obtain a series of Co@Si_x catalysts, where *x* is the Si/Co ratio. The Co@Si_x catalysts with different initial Si/Co ratios of 0.52, 1.48, and 1.87 were synthesized by procedures similar to those used for Co₃O₄@Si_{0.95} and Co@Si_{0.95} catalysts except for changing the amount of TEOS to 20, 60, and 80 mmol.

Synthesis of CoO_x catalyst: The CoO_x catalyst was synthesized following the similar synthesis procedures for Co@Si_x catalysts without using TEOS.

Synthesis of Co/SiO₂ catalyst: 1.2 g of SiO₂ was dispersed into 100 mL of aqueous solution containing 20 mmol of Co(NO₃)₂·6H₂O and 100 mmol of CO (NH₂)₂, followed by stirring at 80 °C for 4 h, then the precipitate was separated by filtration and washed with deionized water. After drying at 100 °C overnight, calcining at 400 °C in air for 4 h and reducing in flowing hydrogen (10% H₂/Ar, 60 mL/min) for 3 h at 600 °C, the Co/SiO₂ catalyst was obtained.

Synthesis of Co@Si_{0.95}-Na catalyst: 1.0 g of Co@Si_{0.95} catalyst was dispersed into 100 mL of aqueous solution containing 1 mmol of NaOH, followed by stirring at room temperature for 3 h. Then the catalyst was separated by filtration and washed with deionized water. After drying at 100 °C overnight and reducing in flowing hydrogen (10% H₂/Ar, 60 mL/min) for 3 h at 600 °C, the Co@Si_{0.95}-Na catalyst was obtained.

Characterization. X-ray diffraction (XRD) patterns were collected on a Rigaku D/MAX 2550 diffract meter with Cu K α radiation ($\lambda = 1.5406$ Å). The Fourier-transform IR (FT-IR) spectra were recorded on a Bruker Vector 22 in the range of 4000–400 cm⁻¹. The composition of Co@Si_x catalysts was measured by an inductively coupled plasma (ICP) analysis (Perkin-Elmer 3300DV). Transmission electron microscopy (TEM), scanning transmission electron microscopy (STEM) images and selected area electron diffraction (SAED) were obtained on a JEM-2100F electron microscopy with an acceleration voltage of 200 kV. X-ray photoelectron spectra (XPS) of the samples were recorded using a Kratos AXIS SUPRA with Al K α X-ray radiation as the X-ray source. The binding energies were calibrated on the basis of the C 1s (284.8 eV) peak. X-Ray absorption near edge structure (XANES) and extended X-ray absorption fine structure (EXAFS) measurements at the Co K-edge were made at beamline 8-ID at the National Synchrotron Light Source II (NSLS II) at Brookhaven National Laboratory and BL14W1 beamline of the Shanghai Synchrotron Radiation Facility. The O K-edge soft X-ray absorption spectra (XAS) were measured at the BL12B-a beamline of the National Synchrotron Radiation Laboratory (NSRL). H₂-temperature-programmed reduction (H₂-TPR) was performed with a Finesorb-3010.

In situ DRIFTS characterization. DRIFTS were recorded using a Thermo Fisher Nicolet iS50 FT-IR spectrometer equipped with a MCT/A detector and ZnSe windows and a high temperature reaction chamber under ambient pressure. In a typical run, 50 mg of solid sample was loaded into the chamber and pretreated at 200 °C for 30 min in flowing Ar (20 mL/min). Then, the chamber was adjusted to the desired temperature (250 °C), and CO₂ (10% CO₂ in Ar) was flowed through the sample for 30 min. After removing the physically adsorbed CO₂ by pure Ar gas, the DRIFTS signals were recorded (Supplementary Fig. 40).

In order to observe the reaction intermediates on the catalyst surface, the similar procedures were repeated except using mixed gas of CO₂ and H₂. CO₂ (10% CO₂ in Ar) and H₂ (10% H₂ in Ar) with controlled ratios were continuously introduced to the chamber (40 mL/min) at 350 °C, and the data were collected (Figs. 4a, b and Supplementary Figs. 41–43).

In situ Raman characterization. Raman spectra were recorded using a HR800 Raman spectrometer equipped with an Ar excitation source ($\lambda = 514.532$ nm). The hydrogen was introduced into the sample chamber (10% H₂ in Ar) to reduce the solid samples at desired temperatures (25–600 °C) for 30 min, then the spectra were collected (Supplementary Fig. 31). For investigating the CO₂ adsorption, the samples were pretreated with H₂ at 250 °C and then the feed gases were introduced. For investigating the reaction on the sample, the above-mentioned procedures were repeated except using mixed gas of CO₂ and H₂ (1:3) in the treatment at 250 °C (Supplementary Fig. 45).

In situ XPS characterization. XPS spectra were recorded using a SPECS NAP-XPS with a monochromatic Al K α source. The exposure to reaction gas was done by backfilling the NAP-XPS chamber. The binding energies were calibrated on the basis of the C 1s (284.8 eV) peak. In a typical run, 50 mg of solid sample was molded in advance and fixed in the chamber, then the sample chamber was evacuated. The blank XPS spectra were collected at 25 °C, followed by reducing the solid samples at controlled temperatures (300, 400, 500, 600, and 650 °C) in a hydrogen atmosphere (pure H₂, 0.1 mbar) for 10 min, then the data were collected to identify the changes of Co and O (Fig. 31 and Supplementary Figs. 23, 27 and 28).

For investigating the CO₂ adsorption on the samples, the chamber was vacuumed again to eliminate the excess hydrogen, and another feed gas (pure CO₂, 1.0 mbar) was introduced for 10 min at 250 °C, the XPS spectra were recorded in the meanwhile. For investigating the CO₂ hydrogenation reaction on the samples, the above-mentioned procedures were repeated except using mixed gas of CO₂ and H₂ with the desired gas ratio (CO₂:H₂ = 3:1, 1:1 and 1:3, total pressure was 1.2 mbar) in the treatment at 250 °C (Fig. 4c and Supplementary Figs. 44 and 46). In the end, 1.0 mbar of hydrogen was introduced to regain a fresh sample. The XPS spectra were recorded following the above-mentioned procedures. The CO₂ hydrogenation activity of the catalysts was further studied at a low hydrogen pressure. A mixed gas containing 0.1 mbar of hydrogen and 1.0 mbar of CO₂ was introduced into the chamber for 5 min. Then the gas was switched off and slowly evacuated from the chamber, and the XPS spectra were recorded (Supplementary Figs. 47 and 48).

CO₂ hydrogenation. The CO₂ hydrogenation was carried out in a tubular fixed-bed continuous-flow reactor equipped with gas chromatography (GC). 0.2 g of catalyst (40–60 mesh) was diluted with 0.4 g of quartz sand (40–60 mesh) in the catalyst bed. The reaction was conducted under reaction conditions of 1.0–4.0 MPa, 260–380 °C, V(H₂:CO₂:Ar) = 50:25:25, 60:20:20, or 76:19:5, GHSV = 3000–12,000 mL/g h. The emission gas (Ar, CO, CH₄, CO₂, and C₂₊ hydrocarbons) from the reactor was maintained at 130 °C and immediately transported to the sample valve of a Fu Li-9790 GC equipped with a thermal conductivity detector (TCD) and a Fu Li-9790 GC equipped with a flame ionization detector (FID). The liquid phase products (CH₃OH) were collected in a cold trap and then analyzed with a Fu Li-9790 GC equipped with FID, with benzyl alcohol as an internal standard. Error bounds for the conversion and selectivity are $\pm 0.3\%$ and $\pm 0.5\%$, respectively.

Data availability

The source data underlying Figs. 2–4 are provided as a Source Data file. The other primary data that support the plots within this paper and findings of this study are available from the corresponding author on reasonable request.

Received: 15 October 2019; Accepted: 4 February 2020;

Published online: 25 February 2020

References

- Matsubu, J. C. et al. Adsorbate-mediated strong metal–support interactions in oxide-supported Rh catalysts. *Nat. Chem.* **9**, 120–127 (2017).
- Li, S. et al. Tuning the selectivity of catalytic carbon dioxide hydrogenation over iridium/cerium oxide catalysts with a strong metal–support interaction. *Angew. Chem. Int. Ed.* **56**, 10761–10765 (2017).
- Gao, P. et al. Direct production of lower olefins from CO₂ conversion via bifunctional catalysis. *ACS Catal.* **8**, 571–578 (2018).
- Li, Z. et al. Highly selective conversion of carbon dioxide to lower olefins. *ACS Catal.* **7**, 8544–8548 (2017).
- He, Z. et al. Water-enhanced synthesis of higher alcohols from CO₂ hydrogenation over a Pt/Co₃O₄ catalyst under milder conditions. *Angew. Chem. Int. Ed.* **55**, 737–741 (2016).
- Bai, S. et al. Highly active and selective hydrogenation of CO₂ to ethanol by ordered Pd–Cu nanoparticles. *J. Am. Chem. Soc.* **139**, 6827–6830 (2017).
- Wang, L. et al. Selective hydrogenation of CO₂ to ethanol over cobalt catalysts. *Angew. Chem. Int. Ed.* **57**, 6104–6108 (2018).
- Chen, Y. et al. Optimizing reaction paths for methanol synthesis from CO₂ hydrogenation via metal–ligand cooperativity. *Nat. Commun.* **10**, 1885 (2019).
- Wei, J. et al. Directly converting CO₂ into a gasoline fuel. *Nat. Commun.* **8**, 15174 (2017).
- He, Z. et al. Synthesis of liquid fuel via direct hydrogenation of CO₂. *Proc. Natl Acad. Sci. USA* **116**, 12654–12659 (2019).
- Gao, P. et al. Direct conversion of CO₂ into liquid fuels with high selectivity over a bifunctional catalyst. *Nat. Chem.* **9**, 1019–1024 (2017).
- Tian, P., Wei, Y., Ye, M. & Liu, Z. Methanol to olefins (MTO): from fundamentals to commercialization. *ACS Catal.* **5**, 1922–1938 (2015).
- Breen, J., Burch, R., Kulkarni, M., Collier, P. & Golunski, S. Enhanced para-xylene selectivity in the toluene alkylation reaction at ultralow contact time. *J. Am. Chem. Soc.* **127**, 5020–5021 (2005).
- Lin, L. et al. Low-temperature hydrogen production from water and methanol using Pt/ α -MoC catalysts. *Nature* **544**, 80–83 (2017).
- Steele, B. C. H. & Heinzel, A. Materials for fuel-cell technologies. *Nature* **414**, 345–352 (2001).
- Yang, X. et al. Low pressure CO₂ hydrogenation to methanol over gold nanoparticles activated on a CeO_x/TiO₂ interface. *J. Am. Chem. Soc.* **137**, 10104–10107 (2015).
- Martin, O. et al. Indium oxide as a superior catalyst for methanol synthesis by CO₂ hydrogenation. *Angew. Chem. Int. Ed.* **55**, 6261–6265 (2016).
- Studt, F. et al. Discovery of a Ni–Ga catalyst for carbon dioxide reduction to methanol. *Nat. Chem.* **6**, 320–324 (2014).
- Fiordaliso, E. M. et al. Intermetallic GaPd₂ nanoparticles on SiO₂ for low-pressure CO₂ hydrogenation to methanol: catalytic performance and *in situ* characterization. *ACS Catal.* **5**, 5827–5836 (2015).
- Wang, J. et al. A highly selective and stable ZnO–ZrO₂ solid solution catalyst for CO₂ hydrogenation to methanol. *Sci. Adv.* **3**, e1701290 (2017).
- Li, C. S. et al. High-performance hybrid oxide catalyst of manganese and cobalt for low-pressure methanol synthesis. *Nat. Commun.* **6**, 6538 (2015).
- Behrens, M. et al. The active site of methanol synthesis over Cu/ZnO/Al₂O₃ industrial catalysts. *Science* **336**, 893–897 (2012).
- Kuld, S. et al. Quantifying the promotion of Cu catalysts by ZnO for methanol synthesis. *Science* **352**, 969–974 (2016).
- Kattel, S., Ramírez, P. J., Chen, J. G., Rodriguez, J. A. & Liu, P. Active sites for CO₂ hydrogenation to methanol on Cu/ZnO catalysts. *Science* **355**, 1296–1299 (2017).
- Lunkenbein, T. et al. Bridging the time gap: a copper/zinc oxide/aluminum oxide catalyst for methanol synthesis studied under industrially relevant conditions and time scales. *Angew. Chem. Int. Ed.* **55**, 12708–12712 (2016).
- Larmier, K. et al. CO₂-to-methanol hydrogenation on zirconia-supported copper nanoparticles: reaction intermediates and the role of the metal–support interface. *Angew. Chem. Int. Ed.* **56**, 2318–2323 (2017).
- Graciani, J. et al. Highly active copper–ceria and copper–ceria–titania catalysts for methanol synthesis from CO₂. *Science* **345**, 546–550 (2014).
- Kattel, S., Yan, B., Yang, Y., Chen, J. G. & Liu, P. Optimizing binding energies of key intermediates for CO₂ hydrogenation to methanol over oxide-supported copper. *J. Am. Chem. Soc.* **138**, 12440–12450 (2016).
- Yue, H. et al. A copper-phyllsilicate core–sheath nanoreactor for carbon–oxygen hydrogenolysis reactions. *Nat. Commun.* **4**, 2339 (2013).
- Prieto, G., Zečević, J., Friedrich, H., de Jong, K. P. & de Jongh, P. E. Towards stable catalysts by controlling collective properties of supported metal nanoparticles. *Nat. Mater.* **12**, 34–39 (2013).
- Zhang, Q., Kang, J. & Wang, Y. Development of novel catalysts for Fischer–Tropsch synthesis: tuning the product selectivity. *ChemCatChem* **2**, 1030–1058 (2010).
- Xie, X., Li, Y., Liu, Z. Q., Haruta, M. & Shen, W. Low-temperature oxidation of CO catalysed by Co₃O₄ nanorods. *Nature* **458**, 746–749 (2009).
- Hagen, S. et al. Ammonia synthesis with barium-promoted iron–cobalt alloys supported on carbon. *J. Catal.* **214**, 327–335 (2003).
- Cao, A. et al. Mechanistic insights into the synthesis of higher alcohols from syngas on CuCo alloys. *ACS Catal.* **8**, 10148–10155 (2018).
- Yang, C. et al. The interplay between structure and product selectivity of CO₂ hydrogenation. *Angew. Chem. Int. Ed.* **58**, 11242–11247 (2019).
- Flytzani-Stephanopoulos, M. & Gates, B. C. Atomically dispersed supported metal catalysts. *Annu. Rev. Chem. Biomol. Eng.* **3**, 545–574 (2012).
- Li, J. et al. Enhanced CO₂ methanation activity of Ni/anatase catalyst by tuning strong metal–support interactions. *ACS Catal.* **9**, 6342–6348 (2019).
- Lunkenbein, T., Schumann, J., Behrens, M., Schlögl, R. & Willinger, M. G. Formation of a ZnO overlayer in industrial Cu/ZnO/Al₂O₃ catalysts induced by strong metal–support interactions. *Angew. Chem. Int. Ed.* **54**, 4544–4548 (2015).
- Wang, Z. Q. et al. High-performance and long-lived Cu/SiO₂ nanocatalyst for CO₂ hydrogenation. *ACS Catal.* **5**, 4255–4259 (2015).
- Yin, X. J. et al. Preparation and characterization of core–shell structured Co/SiO₂ nanosphere. *J. Alloy. Compd.* **479**, 372–375 (2009).

41. Saib, A. M., Borgna, A., van de Loosdrecht, H., van Berge, P. J. & Niemantsverdriet, J. W. XANES study of the susceptibility of nano-sized cobalt crystallites to oxidation during realistic Fischer–Tropsch synthesis. *Appl. Catal. A* **312**, 12–19 (2006).
42. Wang, J., Zhou, J., Hu, Y. & Regier, T. Chemical interaction and imaging of single Co₃O₄/graphene sheets studied by scanning transmission X-ray microscopy and X-ray absorption spectroscopy. *Energy Environ. Sci.* **6**, 926–934 (2013).
43. Zhong, L., Chen, D. & Zafeiratou, S. A mini review of *in situ* near-ambient pressure XPS studies on non-noble, late transition metal catalysts. *Catal. Sci. Technol.* **9**, 3851–3867 (2019).
44. Lin, T. et al. Fischer–Tropsch synthesis to olefins: catalytic performance and structure evolution of Co₂C-based catalysts under a CO₂ environment. *ACS Catal.* **9**, 9554–9567 (2019).
45. Pei, Y. P. et al. High alcohols synthesis via Fischer–Tropsch reaction at cobalt metal/carbide interface. *ACS Catal.* **5**, 3620–3624 (2015).
46. Yang, C., Zhao, H., Hou, Y. & Ma, D. Fe₃C₂ nanoparticles: a facile bromide-induced synthesis and as an active phase for Fischer–Tropsch synthesis. *J. Am. Chem. Soc.* **134**, 15814–15821 (2012).
47. Yao, S. et al. Reconstruction of the wet chemical synthesis process: the case of Fe₃C₂ nanoparticles. *J. Phys. Chem. C* **121**, 5154–5160 (2017).
48. Kim, Y., Trung, T. S. B., Yang, S., Kim, S. & Lee, H. Mechanism of the surface hydrogen induced conversion of CO₂ to methanol at Cu(111) step sites. *ACS Catal.* **6**, 1037–1044 (2016).
49. Fisher, I. A. & Bell, A. T. *In-situ* infrared study of methanol synthesis from H₂/CO₂ over Cu/SiO₂ and Cu/ZrO₂/SiO₂. *J. Catal.* **172**, 222–237 (1997).
50. Kattel, S. et al. CO₂ Hydrogenation over oxide-supported PtCo catalysts: the role of the oxide support in determining the product selectivity. *Angew. Chem. Int. Ed.* **55**, 7968–7973 (2016).
51. Mudiyansele, K. et al. Importance of the metal–oxide interface in catalysis: *in situ* studies of the water–gas shift reaction by ambient-pressure X-ray photoelectron spectroscopy. *Angew. Chem. Int. Ed.* **52**, 5101–5105 (2013).
52. Kattel, S., Liu, P. & Chen, J. G. Tuning selectivity of CO₂ hydrogenation reactions at the metal/oxide interface. *J. Am. Chem. Soc.* **139**, 9739–9754 (2017).
53. Shustorovich, E. & Bell, A. T. Analysis of CO hydrogenation pathways using the bond-order-conservation method. *J. Catal.* **113**, 341–352 (1988).
54. Cheng, J. et al. Density functional theory study of iron and cobalt carbides for Fischer–Tropsch synthesis. *J. Phys. Chem. C* **114**, 1085–1093 (2010).

Acknowledgements

This work was supported by the National Key Research and Development Program of China (2018YFB0604801), National Natural Science Foundation of China (21822203, 91645105, and 91634201), Natural Science Foundation of Zhejiang Province (LR18B030002), and the Fundamental Research Funds for the Central Universities. The

work at the University of California was supported by the U.S. Department of Energy (DOE), Office of Science, Basic Energy Sciences (BES) Grant FG02-04ER15513. We acknowledge Beamline BL14W1 (Shanghai Synchrotron Radiation Facility), NSRL Beamline BL12B-a (National Synchrotron Radiation Laboratory), and Nano-X (SINANO, CAS). We thank Fang Chen for kindly helping with TEM characterization.

Author contributions

L.X.W. performed the catalyst preparation, characterization, and catalytic tests. E.G. and B.C.G. did the EXAFS/XANES experiments and analysis. Y.W. participated the catalyst preparation and characterization. Z.G. and Y.C. performed in the XPS investigation. X.M. provided helpful discussions. L.W. and F.-S.X. designed this study, analyzed the data, and wrote the paper.

Competing interests

The authors declare no competing interests.

Additional information

Supplementary information is available for this paper at <https://doi.org/10.1038/s41467-020-14817-9>.

Correspondence and requests for materials should be addressed to L.W. or F.-S.X.

Peer review information *Nature Communications* thanks Peng Gao and the other, anonymous, reviewer(s) for their contribution to the peer review of this work. Peer reviewer reports are available.

Reprints and permission information is available at <http://www.nature.com/reprints>

Publisher's note Springer Nature remains neutral with regard to jurisdictional claims in published maps and institutional affiliations.



Open Access This article is licensed under a Creative Commons Attribution 4.0 International License, which permits use, sharing, adaptation, distribution and reproduction in any medium or format, as long as you give appropriate credit to the original author(s) and the source, provide a link to the Creative Commons license, and indicate if changes were made. The images or other third party material in this article are included in the article's Creative Commons license, unless indicated otherwise in a credit line to the material. If material is not included in the article's Creative Commons license and your intended use is not permitted by statutory regulation or exceeds the permitted use, you will need to obtain permission directly from the copyright holder. To view a copy of this license, visit <http://creativecommons.org/licenses/by/4.0/>.

© The Author(s) 2020